Earth and Planetary Science Letters 505 (2019) 20–29

Contents lists available at ScienceDirect

Earth and Planetary Science Letters

www.elsevier.com/locate/epsl

Large effect of water on Fe–Mg interdiffusion in garnet

Baohua Zhang [a,*], Bowen Li [a,b], Chengcheng Zhao [c], Xiaozhi Yang [d]

[a] Key Laboratory for High-Temperature and High-Pressure Study of the Earth's Interior, Institute of Geochemistry, Chinese Academy of Sciences, Guiyang 550081, China
[b] University of Chinese Academy of Sciences, Beijing 100049, China
[c] Institute for Planetary Materials, Okayama University, Misasa, Tottori 682-0193, Japan
[d] State Key Laboratory for Mineral Deposits Research, School of Earth Sciences and Engineering, Nanjing University, Nanjing 210023, China

ARTICLE INFO

Article history:
Received 19 January 2018
Received in revised form 1 October 2018
Accepted 12 October 2018
Available online 23 October 2018
Editor: J. Brodholt

Keywords:
Fe–Mg interdiffusion
garnet
water
point defects
closure temperature

ABSTRACT

The effect of water on the kinetics of Fe–Mg interdiffusion in garnet was investigated at 3 GPa and 1373–1673 K using diffusion couples of pyrope and almandine aggregates, over a wide range of water content (C_{H_2O}) from <7 up to ~1260 wt. ppm. Diffusion profiles were measured by electron microprobe, and the obtained data were fitted by the Boltzmann–Matano equation. Our results show that Fe–Mg interdiffusion coefficient (D_{Fe-Mg}) is nearly independent of the composition of garnet over a wide range of Fe/Mg ratios (with X_{Fe} ranging from 0 to 1). The determined D_{Fe-Mg} can be described by the following Arrhenius relation: D_{Fe-Mg} $(m^2/s) = D_0 C^r_{H_2O} \exp(-\Delta H/RT)$, where $\log(D_0) = -1.70 \pm 0.50$, $r = 1.38 \pm 0.06$, and $H = 310 \pm 33$ kJ/mol. The exponent r of 1.38 implies the incorporation mechanism of water is hydrogen associated with metal and partly silicon vacancies to form neutral point defect complexes. While at the same time, it also suggests a profound role of water in enhancing the Fe–Mg interdiffusion in garnet. With increasing water content from 100 to 1260 wt. ppm H_2O, the Fe–Mg inter-diffusivity is enhanced by about two orders of magnitude, comparable to the effect of temperature increased by about 300 °C under dry condition. Such large effect of water on the kinetics of garnet is expected to have important implications for evaluating the closure temperature of available geospeedometry and geothermometry.

1. Introduction

The diffusion behavior of Fe–Mg in constitutive mantle minerals largely influences the timescales and thermodynamics of a series of mantle processes including magma ascent, magma mixing, cooling of lava flows, and heating or cooling of rocks (Ganguly, 2002). Garnet is an important rock-forming mineral occurring in various igneous and metamorphic rocks in the crust and mantle of the Earth. In the shallow upper mantle, the volume fraction of garnet is only up to ~15 vol%. While in the transition zone, the fraction reaches ~40 vol% for a pyrolite composition mantle and ~60 vol% for a piclogite composition mantle, due to the progressive transformation of pyroxenes into garnet with increasing depth (Irifune and Ringwood, 1987). Therefore, Fe–Mg interdiffusion in garnet is expected to play a crucial role in influencing various thermodynamic processes in mantle, owing to its large volume fraction.

Structurally bound water as hydroxyl groups in the lattice of silicate minerals is thought to have a significant effect on the transport properties of mantle minerals, including diffusion (Kubo et al., 2004; Hier-Majumder et al., 2005), rheology (Mei and Kohlstedt, 2000; Xu et al., 2013; Faul et al., 2016) and electrical conductivity (e.g., Yoshino et al., 2006; Wang et al., 2006; Yang, 2012; Zhang et al., 2012). For garnet with various compositions, extensive data on Fe–Mg interdiffusion have been reported in the past decades (e.g., Elphick et al., 1985; Chakraborty and Ganguly, 1992; Ganguly et al., 1998a; Freer and Edwards, 1999; Perchuk et al., 2009; Borinski et al., 2012). Although natural garnet samples in those studies were expected to have some dissolved water, the water content was not measured and the effect of water was usually included in the retrieved values of diffusion coefficients under nominally anhydrous conditions (Dohmen and Milke, 2010). Previous studies on the interdiffusion of Fe–Mg in olivine (Hier-Majumder et al., 2005) and wadsleyite (Kubo et al., 2004) demonstrated that water enhanced greatly the interdiffusivity, although the effect of water on diffusion has been questioned by recent studies for Si and O diffusion in forsterite (Fei et al., 2013, 2014) which suggested a negligible influence of water. The absence of any available data for the possible effect of minor amount of water on Fe–Mg interdiffusion in garnet may

* Corresponding author.
E-mail address: zhangbaohua@vip.gyig.ac.cn (B. Zhang).

https://doi.org/10.1016/j.epsl.2018.10.015
0012-821X/

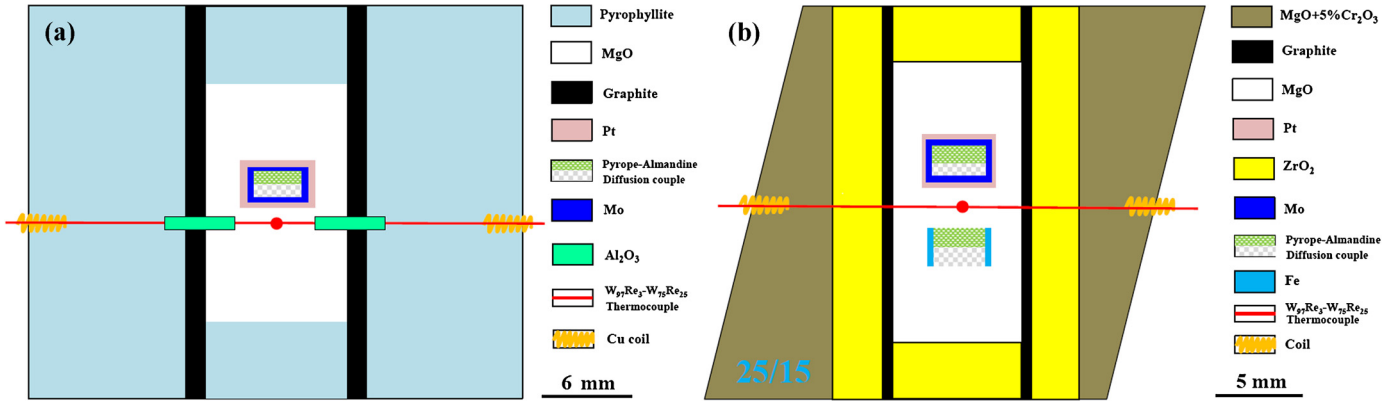

Fig. 1. Cell assembly for the high pressure diffusion experiments in YJ-3000t (a) and Kawai-1000t (b) multianvil apparatus.

have been caused by the technical difficulties in performing diffusion experiment under hydrous conditions. Therefore, a systematic quantitative experimental study is necessary.

In this report, we have for the first time systematically measured the Fe–Mg interdiffusion coefficients in garnet at 3 GPa and 1373–1673 K and over a wide range of water content (C_{H_2O}) from <7 up to $\sim$1260 wt. ppm H_2O. The results show that the Fe–Mg interdiffusion is strongly enhanced by water. With the obtained data, we provide further constraints on Fe–Mg exchange temperatures of garnet-involving geothermometers.

2. Experimental and analytical methods

2.1. Sample preparation

The starting materials of almandine ($Fe_3Al_2Si_3O_{12}$) and pyrope ($Mg_3Al_2Si_3O_{12}$) garnet were prepared from oxide mixture of Fe_2O_3, SiO_2 and Al_2O_3 or MgO, SiO_2 and Al_2O_3 according to the following procedures. The oxide powders were dried at 1273 K for 8 h, and then mixed in an agate mortar for 2 h. To synthesize dry almandine or pyrope garnet, almandine or pyrope glass was first synthesized by melting its corresponding powder mixture at 1873 K in air using a Pt basket and then quenched in water. After that, the glass was finely ground and pressed into pellets again. The pellets were heated at ambient pressure and 1473 K for 2 h in a gas mixing furnace with oxygen fugacity controlled close to the Mo–MoO_2 (MMO) buffer pairs, and then quenched in water. Finally, the obtained finely ground powder was loaded into a Fe capsule at 3 GPa and 1473 K for a few hours with oxygen fugacity buffered by the Fe–FeO (IW) buffer pairs.

Water-doped almandine and pyrope garnet aggregates were synthesized in a slightly different way. First, mildly Al-deficient dry glasses were prepared using the similar procedures above. Then, the glasses were mixed with certain amounts of aluminum hydroxide powder, served as water source and also used to make up for the weak Al-deficiency. The mixtures were loaded into Mo-lined Pt capsules so that the oxygen fugacity was close to MMO. The Pt capsules were welded under liquid nitrogen cooled environment. Finally, the materials were annealed at 3 GPa and 1373–1573 K for a few hours.

High pressure experiments were carried out with a YJ-3000t press and a 1000 ton Kawai type multi-anvil apparatus, both installed at Guiyang Institute of Geochemistry, Chinese Academy of Sciences, China. For the YJ-3000t press, high pressure was generated by six first-stage cubic tungsten carbide anvils. A pyrophyllite cube and a graphite sleeve were used as pressure-transmitting medium and heater, respectively. Prior to high pressure experiments, the pyrophyllite cube and plug were pre-heated at 1173 K to remove absorbed water. For the Kawai-1000t multi-anvil apparatus, the pressure assembly consists of a Cr_2O_3-doped MgO octahedra, a ZrO_2 thermal insulation sleeve, a graphite cylindrical furnace, and a MgO sleeve which insulates the Pt sample capsule from the furnace. Temperatures were monitored using a $W_{97}Re_3$–$W_{75}Re_{25}$ thermocouple and no corrections were applied for pressure effect on thermocouple emf. The pressure was calibrated by the phase transition of Bi (2.5 and 7.7 GPa) at ambient temperature and the phase transition from quartz to coesite at high temperature (Mirwald and Massonne, 1980).

A cooling rate of about 20 °C/min was adopted for both dry and hydrous samples, so that significant cracks in sintered garnet aggregates due to thermal shock could be avoided/minimized. After the sintering, cylinders of 2.0 mm diameter were cored from the recovered samples, and were sectioned to a thickness of 0.3–0.6 mm and then polished with 0.25 μm diamond powder and finally with colloidal silica. These pre-synthesized end-member almandine and pyrope aggregates were used as the starting materials for subsequent interdiffusion experiments.

2.2. Interdiffusion experiments

The diffusion couple method was used for the Fe–Mg interdiffusion experiments between almandine and pyrope aggregates, in a YJ-3000t press using a cubic assembly (Fig. 1a) and a Kawai-1000t double-stage multi-anvil apparatus using a 25/15 octahedral assembly (Fig. 1b). The diffusion experiments at 3 GPa were performed at 1373–1673 K and 1473 K for the dry and water-doped garnets, respectively (Table 1). For experiments on dry samples, the diffusion couples were inserted into a Fe-lined MgO capsule (Fig. 1). For experiments on water-doped samples, the diffusion couples were loaded into Mo–Pt double capsules (Fig. 1), note that caution was paid to the welding of Pt capsules (the capsule was one-end welded and then preheated on a 473 K heating plate, and was welded immediately after loading the sample-inserted Mo capsule). In one experiment (run Z018), two diffusion couples (both water-doped samples with Mo–Pt double capsules and water-undoped samples with Fe-lined MgO capsule) were simultaneously loaded into the same assembly (Fig. 1b).

The diffusion couple was first pressurized at room temperature and then heated to the desired temperature with a ramp rate of 20 °C/s. The fluctuation of temperature was within ±10 °C during the diffusion annealings. After the annealing runs, the samples were quenched to room temperature by shutting off the electric power supply, and the pressure was released slowly. A summary of the experimental conditions is given in Table 1.

Table 1
Summary of experimental conditions and results of Fe–Mg interdiffusion coefficients.

Run no.	T (K)	Time (h)	Diffusion couple	C_{H_2O}[a] (wt. ppm)	C_{H_2O}[b] (wt. ppm)	D_{Fe-Mg} (m^2/s)[c]	D_{Fe-Mg} (m^2/s)[d]	Capsule	G (μm)[g]	G (μm)[h]
1K003	1373	17	Nominally dry	7(3)/9(2)[e]	4(2)/2(1)	$6.14\ (0.19) \times 10^{-19}$	$6.34\ (0.22) \times 10^{-19}$	Fe	6(2.3)/5(2.0)	7(1.9)/6(2.2)
Z018-a	1473	24	Nominally dry	7(3)/9(2)	3(1)/n.d.[f]	$2.81\ (0.21) \times 10^{-18}$	$2.66\ (0.41) \times 10^{-18}$	Fe	7(2.1)/6(1.8)	8(2.0)/7(1.5)
Z029	1573	12	Nominally dry	7(3)/9(2)	3(2)/4(1)	$1.33\ (0.14) \times 10^{-17}$	$1.52\ (0.18) \times 10^{-17}$	Fe	7(2.4)/6(1.3)	8(2.5)/7(1.9)
1K004	1673	8	Nominally dry	7(3)/9(2)	n.d./3(2)	$5.87\ (0.15) \times 10^{-17}$	$6.07\ (0.26) \times 10^{-17}$	Fe	8(2.6)/9(2.4)	9(2.5)/10(2.6)
Z058	1473	28	Nominally dry	7(3)/9(2)	4(2)/5(1)	$3.24\ (0.24) \times 10^{-18}$	$3.12\ (0.34) \times 10^{-18}$	Ni	7(2.6)/8(2.0)	8(2.3)/9(2.5)
Z016	1473	12	Wet	1283(78)/1200(45)	1260(58)/1220(62)	$1.53\ (0.36) \times 10^{-14}$	$1.52\ (0.33) \times 10^{-14}$	Mo	15(3.3)/12(3.0)	17(4.2)/15(4.8)
Z028	1473	24	Wet	794(71)/810(63)	815(62)/782(46)	$8.82\ (0.24) \times 10^{-15}$	$1.14\ (0.35) \times 10^{-14}$	Mo	13(4.1)/11(3.7)	15(3.9)/13(3.5)
Z018-b	1473	24	Wet	566(64)/523(48)	531(46)/n.d.	$2.01\ (0.12) \times 10^{-15}$	$1.89\ (0.22) \times 10^{-15}$	Mo	12(4.5)/12(4.2)	14(4.7)/13(3.8)
Z017	1473	24	Wet	321(36)/297(30)	302(40)/315(24)	$1.55\ (0.17) \times 10^{-15}$	$1.22\ (0.17) \times 10^{-15}$	Mo	10(3.5)/9(3.2)	12(4.0)/10(3.6)
Z027	1373	24	Wet	106(24)/88(16)	95(18)/n.d.	$2.95\ (0.36) \times 10^{-17}$	$3.20\ (0.45) \times 10^{-17}$	Mo	9(2.5)/7(2.0)	11(3.5)/8(3.0)

All experiments were performed under 3 GPa.
[a] Water content before diffusion annealing measured by FT-IR.
[b] Water content after diffusion annealing measured by FT-IR.
[c] Diffusivity determined by Boltzmann–Matano analysis using Eq. (4) at $X_{Fe} = 0.5$.
[d] Diffusivity determined by Eq. (5).
[e] The range of uncertainties is given in parentheses. The values before and after *forward slash* in each run indicate the water content/or grain size obtained from Mg-rich side and Fe-rich side to the diffusion interface, respectively.
[f] n.d. means the water content was not determined due to the lost sample or the absence of clear infrared absorption peaks.
[g] Denote average grain size (G) before diffusion experiment obtained from intercept method (Mendelson, 1969); over 350 grains were measured for each sample.
[h] Denote average grain size (G) after diffusion experiment obtained from intercept method (Mendelson, 1969); over 350 grains were measured for each sample.

2.3. Sample characterization and diffusion profile measurement

After the runs, the recovered interdiffusion couples were cut in half perpendicular to the interface between the almandine and pyrope couples. One half was mounted in epoxy resin, and polished with diamond powders and colloidal silica. The samples prior to and after the diffusion experiments were examined using X-ray diffraction and Raman spectroscopies, and no other phases than garnets were detected.

Grain size measurements were carried out on the digitized FE-SEM images of the polished section using the intercept method. The variation of intercept length was determined from the measurement of the length between two intercepts (i.e., grain boundary) along the analyzed lines. The average grain size (G) was estimated from the measured average intercept length (L) using the relationship $G = cL$, where c is a constant value of 1.56 (Mendelson, 1969).

The Fe–Mg concentration profiles and element mapping of the diffusion couples were analyzed using an electron probe microanalyzer (EPMA-1600) with an accelerating voltage of 15 kV and a beam current of 5 nA. By using a well-focused beam (1 μm on the sample), multiple diffusion profiles were obtained perpendicular to the initial interface in steps of 1–10 μm, depending on the rate at which the iron concentration changed with distance. The multiple concentration profiles measured in each sample were consistent with each other within the measurement errors.

The other half of each diffusion couple was doubly polished for Fourier transform infrared (FTIR) analysis. To remove surface absorbed water, the sections were heated at ~200 °C in a vacuum oven for 24 h. The unpolarized FTIR spectra were obtained with a Bruker Vertex 70V FTIR spectrometer coupled with a Hyperion 2000 microscope at the School of Earth Sciences and Engineering, Nanjing University. Measurements were carried out by unpolarized radiation with a globar light source, a KBr/Ge beam-splitter and a MCT-A liquid N_2 cooled detector. A total of 128 scans was accumulated for each spectrum at a resolution of 4 cm^{-1} with an aperture size of 50 × 50 μm. The IR spectra were measured on optically clean and inclusion- or fracture-free areas. Water concentrations were calculated by applying the calibration given by Paterson (1982):

$$C_{OH} = \frac{B}{150\xi} \int \frac{H(\upsilon)}{3780 - \upsilon} d\upsilon \tag{1}$$

where B is the density factor, ξ is an orientation factor set to be 1/3, and $H(\upsilon)$ is the absorption coefficient for a given wavenumber υ. The integration was conducted at a wavenumber ranging from 2800 to 3750 cm^{-1}.

2.4. Determining diffusion coefficients

In order to determine the composition-dependent interdiffusion coefficients as a function of iron concentration, the measured diffusion profiles were analyzed by the Boltzmann–Matano method (Matano, 1933; Crank, 1975) which assumes a binary system and an effectively semi-infinite media. For this analysis, the concentration profile was first fitted to a sigmoidal function numerically using an iterative technique:

$$C(x) = A_0 \left(1 - \frac{1}{(1 + \exp(A_1 x + A_2))^{A_3}}\right) \tag{2}$$

where C is the Fe or Mg concentration as a function of distance x, and A_0, A_1, A_2 and A_3 are fitting parameters. Then, the Matano interface was obtained by translating the function with respect to distance x until the following equation is satisfied:

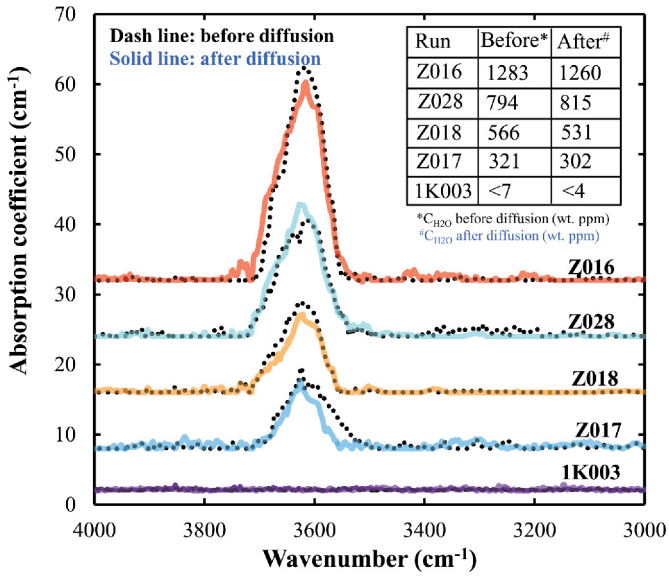

Fig. 2. Unpolarized FT-IR spectra for $Fe_3Al_2(SiO_4)_3$ almandine part of the diffusion couples before and after diffusion anneals. Note that the C_{H_2O} before and after diffusion are essentially the same.

$$\int_{C_1}^{C_2} x\mathrm{d}C = 0 \tag{3}$$

where C_1 and C_2 are the maximum and minimum concentration over the diffusion profiles respectively, which correspond to the initial concentrations of the diffusion couple. The position at $x = 0$ gives the Matano interface. Finally, the Boltzmann–Matano analysis was applied to the fitted concentration profile to obtain the concentration-dependent interdiffusion coefficient:

$$D(C^*) = -\frac{1}{2t}\left(\frac{\mathrm{d}x}{\mathrm{d}C}\right)_{C^*}\int_{C_1}^{C^*} x\mathrm{d}C \tag{4}$$

where $D(C^*)$ is the composition-dependent interdiffusion coefficient at the concentration C^* and t is the run duration of the diffusion experiment. With Eq. (4), we can calculate the integral parts by counting squares $x\mathrm{d}C$. The gradient $(\mathrm{d}x/\mathrm{d}C)_{C^*}$ was calculated from the tangent of the parabola. Uncertainties in the gradient were propagated to estimate the uncertainties on the diffusion coefficient.

In order to illustrate the dependence of diffusivity on Fe concentration, the diffusion profiles were also fitted to the relation for diffusion with a concentration-independent diffusivity, D, for comparison:

$$C(x,t) = \frac{C_1 + C_2}{2} + \frac{C_1 - C_2}{2}\,\mathrm{erf}\left(\frac{x}{2\sqrt{Dt}}\right) \tag{5}$$

3. Results

The average grain sizes in the polycrystalline samples synthesized under hydrous conditions are larger than those in the dry ones, suggesting a water-enhanced grain growth during the runs. However, no significant changes in grain size during the diffusion annealings were observed for both the nominally dry and water-doped diffusion couples (Table 1).

Fig. 2 shows representative unpolarized FTIR spectra of almandine before and after diffusion annealing. The spectra exhibit a broad asymmetric band centered around 3630 cm^{-1}, which

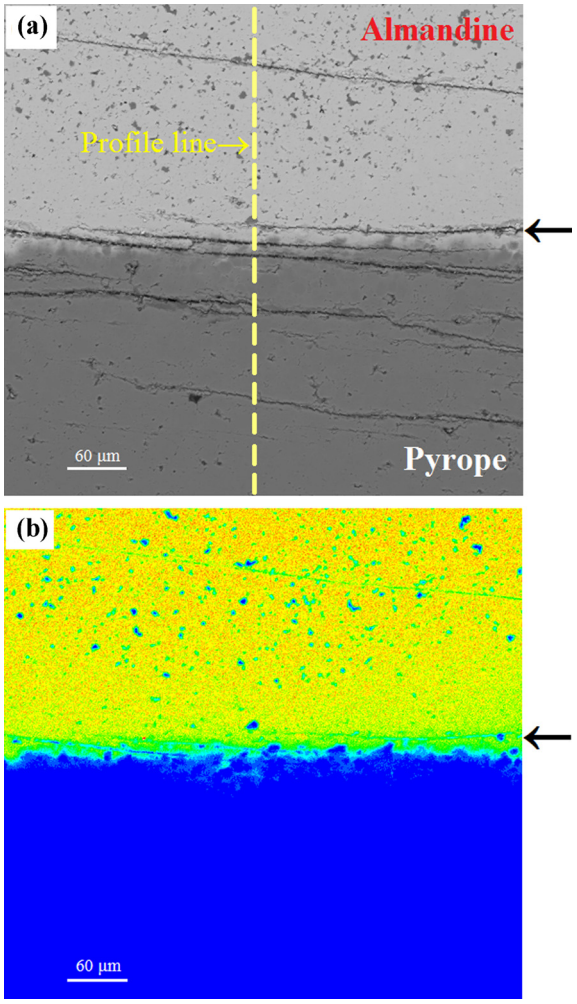

Fig. 3. (a) Backscattered electron image of a garnet diffusion couple (Z018-b). The experiment was annealed at 3 GPa and 1473 K for 24 h under wet condition (~531 weight ppm H_2O). The interface between the two halves of the diffusion couple is indicated by arrow. The position of one of the measured compositional profiles is indicated by a yellow dashed line; this direction is perpendicular to the interface. (b) Element map of Fe in wet diffusion couple of (a). The iron content decreases from *yellow area* (almandine) at the top of the image to *blue area* (pyrope) at the bottom. Note that, a marked diffusion zone can be clearly seen close to the initial interface. (For interpretation of the colors in Fig. 3, the reader is referred to the web version of this article.)

are similar to previous observations for garnet (Mookherjee and Karato, 2010). The water contents in the samples measured before and after the runs are almost the same (Table 1 and Fig. 2), suggesting the absence of significant dehydration or water loss during the diffusion annealing. Noteworthily, several previous studies have demonstrated that a broad peak centered at ~3400 cm^{-1} observed in polycrystalline samples is due to molecular water on grain boundary or fluid inclusions, including natural and synthetic garnet (Katayama et al., 2003; Xia et al., 2005). In this study, no such broad peak in low energy bands was observed in Fig. 2, indicating that the vast majority of water in garnet under our experimental conditions are OH-related species in grains rather than on grain boundaries.

A representative back-scattered electron image of the cross-section of a diffusion couple (Z018-b) is illustrated in Fig. 3a. Fractures observed on the sample were produced probably during the final quench and decompression. Concentration profiles were obtained by avoiding these gaps. Fig. 3b shows an element mapping of Fe in the area of Fig. 3a (Z018-b). Although the initial interface (after polishing of each part of the diffusion couple) was perfectly

flat, the diffusion front is obviously not parallel to the diffusion interface after diffusion experiments. The irregular shape of the interface may have been caused by slight grain growth of garnet during the long-time annealing under high temperature and high pressure. The interface roughness was estimated to be less than 20 μm for hydrous diffusion couples (Fig. 3b).

Fig. 4 shows representative diffusion profiles obtained by EMPA measurements (data points) and fitting curves yielded by the Boltzmann–Matano analyses. It appears that the rate of Fe–Mg interdiffusion in garnet annealed under water-doped conditions is much faster than that under water-free conditions. As a result, the diffusion lengths for the hydrous samples (e.g. ~80 μm in Fig. 4b) are much longer than that for the dry ones (e.g. ~20 μm in Fig. 4a). For nominally dry cases, the Matano interfaces are almost the same as their initial interfaces between the two crystals (e.g. Z029, Fig. 4a), whereas for hydrous samples they move slightly to the Mg-rich side by about 5 μm relatively to their original interfaces (e.g. Z018-b, Fig. 4b).

In general, two major sources of errors should be considered and corrected in the determination of diffusivity from the concentration profiles measured by EPMA. Otherwise the retrieved diffusion coefficient would be larger than its true value if Eqs. (4)–(5) were used to fit the data directly (e.g., Ganguly et al., 1988; Yamazaki and Irifune, 2003; Fei et al., 2013, 2014). One is the convolution effect arising from the spatial averaging effect of microprobe beam (Ganguly et al., 1988). The other is due to the effect of interface roughness after diffusion annealings. The errors of D_{Fe-Mg} determined in the present study are usually smaller than 0.2 log unit (Table A1). Detailed calculation procedures for the uncertainties resulted from both are given in the Appendix.

Fig. 4c displays the obtained D_{Fe-Mg} for water-doped and nominally dry garnets against iron content (X_{Fe}), and the diffusivities for $X_{Fe} = 0.5$ are listed in Table 1. It was reported by Chakraborty (1997) that D_{Fe-Mg} of olivine is strongly dependent on iron content, e.g., the variation is about 3 orders of magnitude between Fa_{100} and Fo_{100}. Similar trends have also been reported for wadsleyite (Kubo et al., 2004) and ferropericlase (Yamazaki and Irifune, 2003; Mackwell et al., 2005; Otsuka and Karato, 2015). In our almandine–pyrope systems, however, the almost symmetric concentration profiles in Fig. 4 suggest similar diffusivities of Fe and Mg and thus little compositional dependence of Fe–Mg diffusion coefficients, i.e. the determined D_{Fe-Mg} are nearly independent of iron contents (Fig. 4c). Therefore, Eqs. (2)–(4) of the Boltzmann–Matano method could be applied to calculate the D_{Fe-Mg} without the corrections for iron concentration.

It should be noted that D_{Fe-Mg} tends to bend upwards when Fe concentration is close to the end-member ($X_{Fe} \rightarrow 0$ or >0.9 in Fig. 4c). This may have been produced from the use of Eq. (2) that is only an approximate fitting to the shape of the interdiffusion profile. As the compositions become progressively closer to those of the starting crystals, the fitted results show gradual deviations. Therefore, the inter-diffusion coefficients determined at the intermediate compositions are more accurate than those near the end-members (Yamazaki and Irifune, 2003; Mackwell et al., 2005). Consequently, the diffusion coefficient at $X_{Fe} = 0.5$ was used for this study. For the sake of comparison, the experimental data were also fitted by Eq. (5) and the results are shown in Fig. 4 and Table 1.

The dependence of temperature and water content on the interdiffusion coefficient could be assessed by using the Arrhenius equation (Hier-Majumder et al., 2005; Fei et al., 2013, 2014; Otsuka and Karato, 2015):

$$D = D_0 C_{H_2O}^r \exp\left(-\frac{\Delta H}{RT}\right) \quad (6)$$

where D_0 is the pre-exponential factor, C_{H_2O} is the water content in wt. ppm H_2O, r is an exponent linked to C_{H_2O}, R is the ideal gas constant, T is the absolute temperature, and ΔH is the activation enthalpy. A global least-square fitting of the diffusion data (Fig. 5a) to Eq. (6) yields D_0, r and ΔH of $10^{-1.70\pm0.50}$ m^2/s, 1.38 ± 0.06, and 310 ± 33 kJ/mol, respectively. The errors were derived from

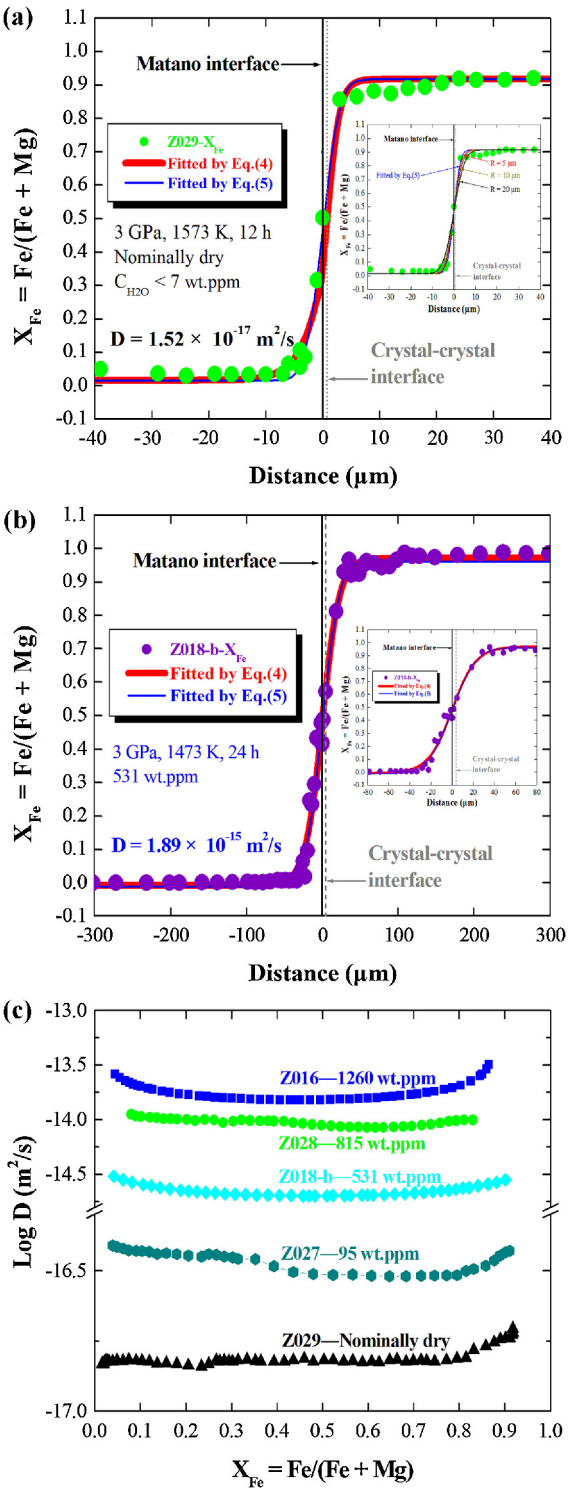

Fig. 4. Representative Fe–Mg interdiffusion profiles as a function of position perpendicular to the original interface in the diffusion couple of nominally dry for Z029 (a) annealed at 1573 K for 12 h and hydrous for Z018-b (b) with 531 wt. ppm H_2O annealed at 1473 K for 24 h. The Matano interface is set at $x = 0$. The solid lines show the Boltzmann–Matano analysis by Eq. (4) and the concentration-independent diffusivity fitted by Eq. (5) to the data. (c) D_{Fe-Mg} as a function of Fe content at 3 GPa and water-bearing and -free conditions using Boltzmann–Matano analyses. Note that, no strong compositional dependence is seen for the D_{Fe-Mg}.

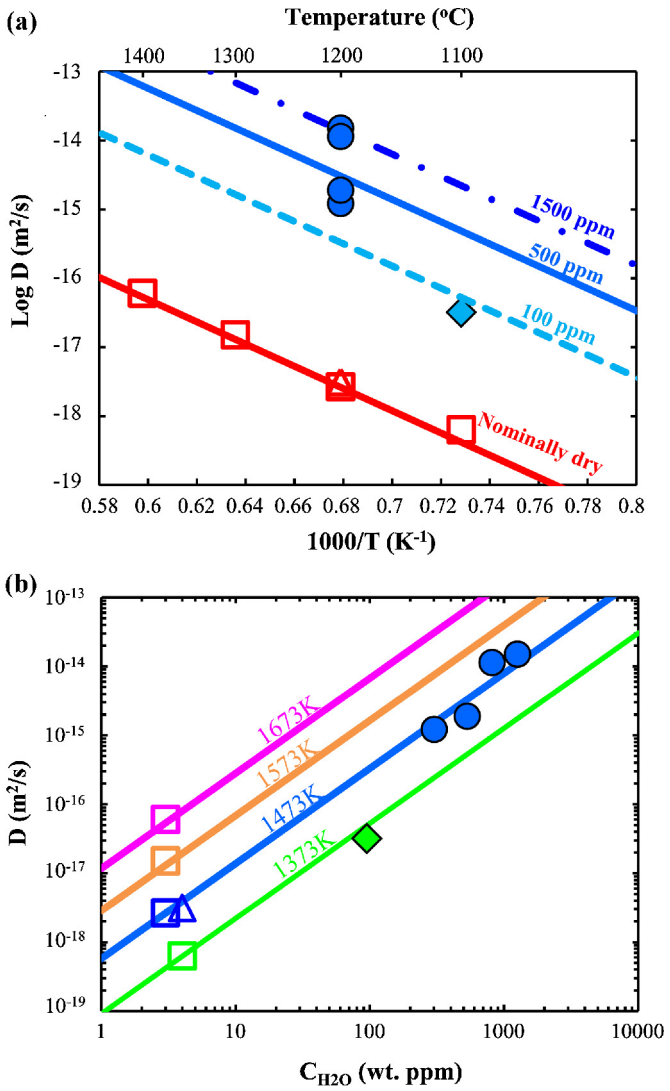

Fig. 5. (a) D_{Fe-Mg} in garnet as a function of reciprocal temperature. (b) D_{Fe-Mg} versus C_{H_2O} at temperature between 1373–1673 K. Note that, open squares denote raw data for each nominally dry diffusion couple and closed symbols indicate raw data for hydrous diffusion couple, respectively. Open triangle denotes the data for run Z058 using Ni capsule (~NNO buffer). Colored lines show D_{Fe-Mg} calculated by data fitting based on Eq. (6) as a function of water content or temperature.

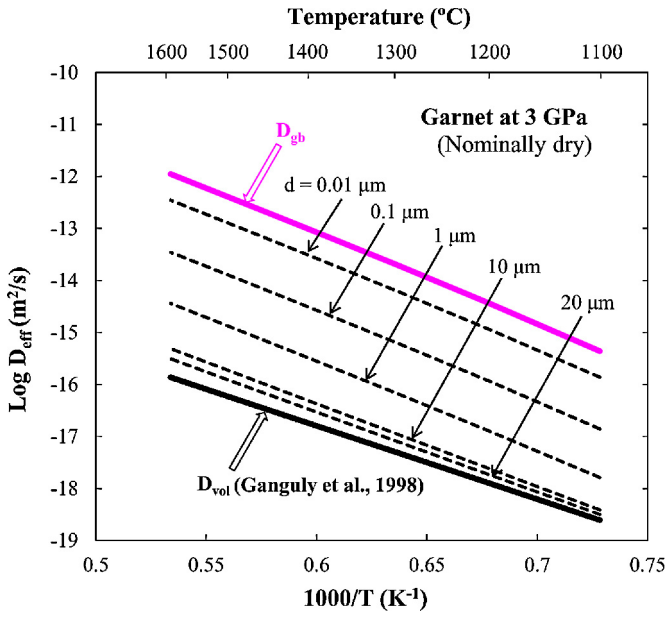

Fig. 6. Grain-size dependence of D_{Fe-Mg} in garnet at 3 GPa calculated based on the relation $D_{eff} = D_{lat} + \pi\delta D_{gb}/G$ using the diffusion rates with different grain size obtained from the nominally dry diffusion couple at constant grain size ~8 μm. The grain boundary width in garnet was assumed to be 1 nm for the estimation of D_{gb}. Mg self-diffusion coefficients in garnet are shown as a function of reciprocal temperature, which is considered to be equal to volume diffusion (Ganguly et al., 1998a).

the propagation of the uncertainties of the diffusion coefficients and the errors associated with the least-squares fitting to the Arrhenius equation.

For experiments annealed under the same temperature, pressure and f_{O_2} conditions, the yielded diffusion coefficients of the water-doped samples systematically increase with increasing water content and are always higher than those of the anhydrous ones. Fig. 5 shows the effects of temperature and water content on the Fe–Mg interdiffusion at 3 GPa and 1373–1673 K with various water contents up to 1260 wt. ppm H_2O. It is clear that water can significantly enhance the Fe–Mg interdiffusivity in garnet. For example, the rate of Fe–Mg interdiffusion in the water-doped sample (Z027 containing only ~100 wt. ppm H_2O) at 1373 K is at least two orders of magnitude faster than that of the anhydrous sample (e.g., 1K003), as shown in Fig. 5a. At a given temperature, $\log D_{Fe-Mg}$ increases approximately linearly with increasing water content (Fig. 5b).

4. Discussion

4.1. Effect of grain size on D_{Fe-Mg}

Significant grain growths were not observed in our recovered samples after the diffusion runs (Table 1). The increment is consistent within 2 μm estimated using the growth kinetics of ugrandite garnets reported by Shtukenberg et al. (2005) due to diffusion-limited process. Therefore, it is possible that the crystal growth of our garnet samples is diffusion-controlled. The changes of grain size in our samples are so small that the effect of grain recrystallization on the measured bulk diffusion coefficients is insignificant because of negligible changes in volume fraction of grain boundaries.

The diffusion in polycrystalline materials involves two mechanisms, diffusion through the volume and diffusion along the grain boundary. Grain-boundary diffusion is in general several orders of magnitude faster than volume diffusion (Ganguly et al., 1998a). Because the diffusion front is not parallel to the diffusion interface after the diffusion experiments (Fig. 3), lattice and grain-boundary diffusion may have both contributed to the obtained diffusion profiles. It is likely that the diffusion in the garnet samples operated in the type-B kinetic regime (Harrison, 1961; Joesten, 1991; Dohmen and Milke, 2010) in the present experiments. However, it is hard to determine the lattice and grain boundary diffusion coefficients separately from the obtained diffusion profiles in Fig. 4, because of the limited spatial resolution of the electron microprobe.

As well known, mass transportation is controlled by the effective diffusion coefficient in polycrystalline materials, $D_{eff} = D_{lat} + \pi\delta D_{gb}/G$ (Raj and Ashby, 1971; Gordon, 1985), where D_{eff} is the effective diffusion coefficient, δ is the grain-boundary width, D_{lat} is the lattice diffusion coefficient, and D_{gb} is the grain-boundary diffusion coefficient. Therefore, D_{gb} could be calculated at $X_{Mg} = 0.5$ for nominally anhydrous garnet using the measured effective diffusion rate with the grain size of ~8 μm (Fig. 6), if we assume the grain boundary width in garnet to be ~1 nm, a value commonly

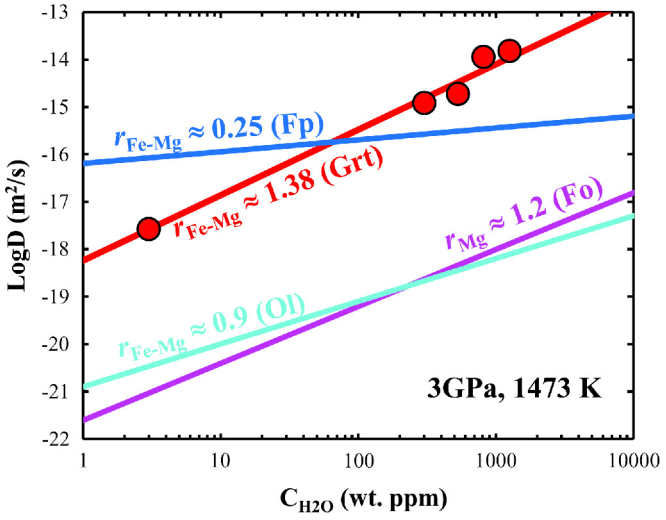

Fig. 7. C_{H_2O} dependences of D^{Grt}_{Fe-Mg} (this study), D^{Ol}_{Fe-Mg} (Hier-Majumder et al., 2005), D^{Fp}_{Fe-Mg} (Otsuka and Karato, 2015), D^{Fo}_{Mg} (Fei et al., 2018) at 3 GPa and 1473 K. All diffusion data are calibrated to 3 GPa and 1473 K using the experimentally reported activation energy and activation volume in each study.

adopted for olivine, oxides and ceramics (Joesten, 1991) and the Mg self-diffusion in garnet single crystal (Ganguly et al., 1998a) by lattice diffusion. The results show that, under the upper mantle conditions, our measured effective diffusion coefficients in polycrystalline garnet are about 2–4 times greater than those reported for lattice diffusion rate by Ganguly et al. (1998a). This suggests that the contribution of grain boundary diffusion to the total diffusive flux is large, although further study is required to quantify the effect of grain boundary diffusion.

4.2. Effect of water on D_{Fe-Mg}

Some researchers proposed recently that the effect of water on oxygen and silicon self-diffusion in forsterite is very limited or even negligible, and that water does not significantly affect the creep rate in olivine assuming the diffusion-controlled deformation mechanism (Fei et al., 2013, 2014). However, a previous Fe–Mg interdiffusion study on olivine has shown that the diffusivity could be significantly enhanced by the presence of structural water, and that an approximately linear relation with an exponent $r = 0.9 \pm 0.3$ could be used to describe the dependence (Hier-Majumder et al., 2005). This is supported by the results of the present study on garnet. At a given pressure and temperature, the rates of Fe–Mg interdiffusion in hydrous garnet are at least one order of magnitude higher than those under anhydrous conditions (Figs. 4–5). The water exponent r of 1.38 ± 0.06 suggests an even larger effect of water for garnet than for olivine. For example, the enhancement in inter-diffusivity by introducing only 100 wt. ppm water in the sample at 1373 K ($D^{Hydrous}_{Fe-Mg} = 3.2 \times 10^{-17}$ m^2/s) is almost identical to that associated with an increase of 300 °C in temperature ($D^{Anhydrous}_{Fe-Mg} = 6.07 \times 10^{-17}$ m^2/s at 1673 K) (Fig. 5). In particular, the influence of water on the Fe–Mg interdiffusion in garnet is the largest among various silicate minerals, since the water exponent r is 0.9 for Fe–Mg interdiffusion in olivine (Hier-Majumder et al., 2005) and 0.25 for Fe–Mg interdiffusion in ferropericlase (Otsuka and Karato, 2015), and 1.1 for Mg lattice diffusion in forsterite (Fei et al., 2018).

Fig. 7 compares the dependence of Fe–Mg interdiffusion on water content in garnet at 3 GPa and 1473 K with other minerals. Under dry conditions ($C_{H_2O} < 4$ weight ppm), the diffusion rates are $D^{Fp}_{Fe-Mg} \gg D^{Grt}_{Fe-Mg} > D^{Ol}_{Fe-Mg} \approx D^{Fo}_{Mg}$. If C_{H_2O} increases by the level of several hundred wt. ppm, which corresponds to conditions in the lower part of the upper mantle or in the subducting slab, the diffusion rates are $D^{Grt}_{Fe-Mg} \gg D^{Fp}_{Fe-Mg} \gg D^{Ol}_{Fe-Mg} \approx D^{Fo}_{Mg}$.

4.3. Diffusion mechanisms

Our experimental results have revealed significant H_2O-enhanced D_{Fe-Mg} in garnet, which would be attributed to dissolution of hydrogen into garnet crystal structure. Theoretical studies demonstrated that water can be incorporated into garnet via a number of different defect mechanisms (Wright et al., 1994; Pigott et al., 2015): (i) $H_2O + 2Fe^{\bullet}_{Me} + 2O^{X}_{O} \rightarrow 2(OH)^{\bullet}_{O} + 2Fe^{X}_{Me} + 1/2O_2$, incorporation of hydrogen by reducing ferric Fe. (ii) $2H_2O + Si^{X}_{Si} + 4O^{X}_{O} \rightarrow [V_{Si}(OH)_4]^{X} + SiO_2$, incorporation of hydrogen by creating silicon vacancies at the tetrahedral site as the hydrogarnet defect $[V_{Si}(OH)_4]^{X}$. (iii) $H_2O + Me^{X}_{Me} + 2O^{X}_{O} \rightarrow [V_{Me}(OH)_2]^{X} + MeO$, incorporation of hydrogen by creating metal vacancies at octahedral and dodecahedral sites as either $[V_{Me}(OH)_2]^{X}$ or $[Me_{Si}(OH)_4]^{X}$.

While structurally incorporated hydrogen can be identified by IR spectroscopy, it is not clear that how the hydrogen atoms are incorporated into garnet structure. To better understand the detailed diffusion mechanism under hydrous conditions, examining the water exponent would be more useful. It is worth noting that, the water exponent in the mechanism (i) yields $D_{Fe-Mg} \propto f^{0.5}_{H_2O}$, which is inconsistent with our result. Our determined water exponent ($r = 1.38$) lies between the mechanisms (ii) ($D_{Fe-Mg} \propto f^{2}_{H_2O}$) and (iii) ($D_{Fe-Mg} \propto f_{H_2O}$), suggesting that cation diffusion in garnet under water-doped conditions might not be controlled by a single mechanism but rather involving both mechanisms. In fact, several previous studies have suggested that the sharp absorption bands in unpolarized FTIR spectra between 3560 and 3670 cm^{-1} result from OH associated with tetrahedral (silicon) or octahedral (metal) vacancies (Katayama et al., 2003; Mookherjee and Karato, 2010), which possibly implied multiple hydrogen incorporation mechanisms.

Since IR data here cannot separate different incorporation mechanisms, the other way is to calculate the formation energy of hydroxyl groups by employing theoretical simulation (for example, first-principle calculation, molecular dynamics) for both bounded and unbounded OH. The OH stretching vibrational properties can be readily determined for each configuration and compared with the experimentally obtained IR spectra, which can be used to constrain diffusion mechanisms and aid interpreting experimental data. Although several theoretical studies have investigated hydrogarnet substitution in grossular (Wright et al., 1994) and majorite garnet (Pigott et al., 2015), unfortunately, the energetics of the incorporation of hydrogen and the OH stretching frequency of the hydroxyl groups in almandine–pyrope solid solution system are still not well understood. Thus in the present experiments, it is hard to distinguish which defect mechanism (i.e., ii and iii) is dominant as well as their relative contributions to Fe–Mg interdiffusion in garnet. Therefore laboratory and theoretical work is required to identify and quantify the detailed mechanisms on enhancement of the diffusivity by water in garnet in future.

In addition, oxygen fugacity is expected to influence diffusion property by changing the defect concentrations through changing of oxidation state of multivalent elements (such as Fe) and of the defect sites in the structure (Ganguly, 2002; Dohmen and Milke, 2010; Zhang, 2017). In present experiments, two different kinds of buffers consisting of Fe capsule (~IW buffer) and Mo capsule (~MMO buffer, which is thought to be maintained an oxygen fugacity close to the IW buffer) were used for nominally anhydrous and hydrous diffusion couple, respectively. In order to check the effect of oxygen fugacity on D_{Fe-Mg} and diffusion mechanism, one additional diffusion experiment (Run no. Z058) was done using a nominally anhydrous diffusion couple, whose duration was

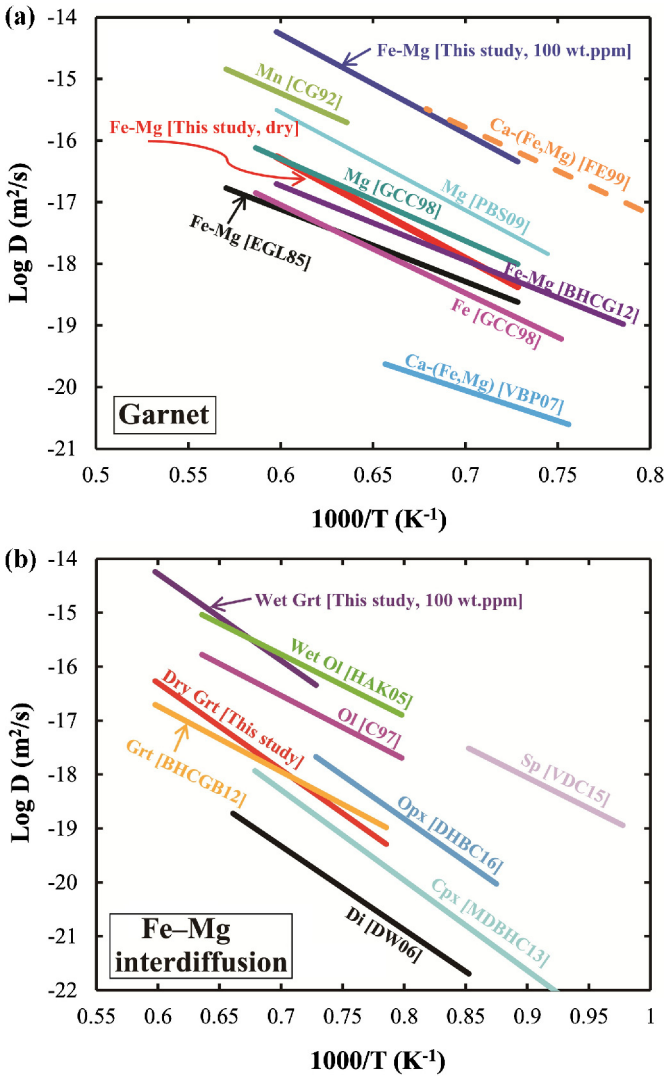

Fig. 8. Comparison of various cations diffusion data in garnet (a) and Fe–Mg interdiffusion in other related minerals (b). Data source: BHCGB12 (Borinski et al., 2012), EGL85 (Elphick et al., 1985), FE99 (Freer and Edwards, 1999), VBP07 (Vielzeuf et al., 2007), PBS09 (Perchuk et al., 2009), GCC98 (Ganguly et al., 1998a), CG92 (Chakraborty and Ganguly, 1992), DHBC16 (Dohmen et al., 2016), MDBHC13 (Müller et al., 2013), DW06 (Dimanov and Wiedenbeck, 2006), C97 (Chakraborty, 1997), HAK05 (Hier-Majumder et al., 2005), VDC15 (Vogt et al., 2015).

28 h and Ni capsule (∼NNO buffer) was used (Table 1). The resultant $D_{\text{Fe–Mg}}$ $\sim 3.12 \times 10^{-18}$ m^2/s is almost identical to that of 2.66×10^{-18} m^2/s under the IW buffered condition in Z018-a (Table 1), which implies that under anhydrous condition Fe–Mg inter-diffusion in garnet has little dependence on oxygen fugacity. Consequently, the influence of oxygen fugacity on defect concentrations and eventually diffusion mechanism is tiny in garnet.

4.4. Comparison with previous studies

In order to discuss the rate-controlling species for garnet, we compare our Fe–Mg diffusion rates with those of various cations (Fe, Mg, Mn, Ca–(Fe, Mg)) (Elphick et al., 1985; Chakraborty and Ganguly, 1992; Ganguly et al., 1998a; Freer and Edwards, 1999; Perchuk et al., 2009; Borinski et al., 2012) obtained from diffusion couple experiments. For the purpose of discussing the rate-controlling species in mantle garnet, the experimental data mentioned here are restricted to Fe–Mg rich, Mn-poor garnets. Fig. 8a shows a summary of the comparisons in the form of an Arrhenius plot without pressure corrections. We note that the diffusion rates of Fe–Mg in hydrous garnet reported in this study are the fastest ones among all the existing data for garnet, which are practically identical to that of Ca–(Fe, Mg) interdiffusion between grossular and almandine single crystals (Freer and Edwards, 1999). Within the experimental temperature range of ∼1173–2073 K and under anhydrous conditions, the Fe–Mg interdiffusivity obtained in this study are close to those of Borinski et al. (2012) but faster than that of Elphick et al. (1985). The D_{Mg} of Ganguly et al. (1998a) are comparable to those reported by Perchuk et al. (2009) and $D_{\text{Fe–Mg}}$ of Borinski et al. (2012). However, these data are respectively around ∼1.0 and ∼1.5 log units lower than the D_{Mg} of Perchuk et al. (2009) and D_{Mn} of Chakraborty and Ganguly (1992), while greater than the $D_{\text{Fe–Mg}}$ of Elphick et al. (1985) and D_{Fe} of Ganguly et al. (1998a). In addition, the interdiffusion coefficients of Ca–(Fe, Mg) in garnet reported by Vielzeuf et al. (2007) are much lower than those obtained by Freer and Edwards (1999) (Fig. 8a), which may be caused by the large compositional dependence of the quasi-binary interdiffusion coefficient between these two experiments. In review of those available data on cation diffusion in garnet, it seems that many factors such as composition, oxygen fugacity, temperature and water content could make inter-diffusion more complex, through affecting the concentration and species of point defects in garnets and eventually the diffusion processes (Zhang, 2017; Li et al., 2018).

Fe–Mg diffusion rates in garnet may be compared with those of other related mantle minerals. As shown in Fig. 8b, the diffusion rates of Fe–Mg in garnet obtained in this study under anhydrous conditions are similar to the rates of diffusion in orthopyroxene (Dohmen et al., 2016) and garnets (Borinski et al., 2012), somewhat faster than the rates in clinopyroxene (Müller et al., 2013), and lower than the diffusion rates in olivine (Chakraborty, 1997) and spinel (Vogt et al., 2015). While the rates of Fe–Mg diffusion in hydrous garnet are almost identical to the diffusion rates in hydrous olivine (Hier-Majumder et al., 2005) and dry spinel (Vogt et al., 2015), the diffusion rates of Fe–Mg in diopside (Dimanov and Wiedenbeck, 2006) are the lowest among these reported data in Fig. 8b. However, the diffusion rates of Fe–Mg in water-bearing minerals are much faster than those in water-free ones.

4.5. Implications for geospeedometry and geothermometry

Garnet is the most important mineral in the study of p–T–t history of metamorphic rocks. Since garnet is isotropic, whose diffusion has no directional dependence, it has a practical advantage in modeling frozen compositional profiles for geospeedometry. In addition, the temperature dependence of Fe–Mg diffusion coefficients between garnet and coexisting minerals such as spinel, orthopyroxene and clinopyroxene, provides constraints on some of the most widely used geothermometers (Schwandt et al., 1995; Ganguly and Tirone, 1999; Ganguly, 2002; Borinski et al., 2012; Müller et al., 2013).

The inter-diffusion data in this study can be used to estimate closure temperature and cooling rates associated with compositional zoning in garnet. During cooling after thermal metamorphism, the composition of garnet can be modified in response to changing conditions until temperature drops to closure temperature, T_C, below which volume diffusion is not a viable process and the composition was fixed. The closure temperature T_C earlier proposed by Dodson (1973) can be defined through the relation:

$$\frac{\Delta H}{RT_C} = \ln\left(-\frac{ART_C^2 D_0}{a^2 \Delta H \frac{dT}{dt}}\right) \tag{7}$$

where ΔH is the activation enthalpy of diffusion, R is the gas constant, A is a geometric factor (which is equal to 55 for spheres), D_0 is the diffusion pre-exponential factor, a is the radius of a spherical

grain, and $\frac{dT}{dt}$ is the cooling rate (a negative value). Using Eq. (7) and diffusion parameters determined from Eq. (6) in this study, significantly different closure temperatures for a given cooling rate under dry and wet conditions are obtained as is illustrated in Fig. 9a. For example, under water-free conditions, a 5 mm diameter garnet cooling at a rate of 100 °C/Ma has a closure temperature of 990 °C, whereas under water-bearing conditions (even assume it contains only 100 wt. ppm H_2O), it is reduced to 830 °C. Such contrast reflects significant temperature resetting during cooling if garnets contain small amount of water.

However, the derivation of the classical Dodson formulation (7) rests on several assumptions (Dodson, 1973, 1986). Among those one condition that at peak temperature T_0, the mineral grain is not retentive of the diffusing species over short timescales, makes T_C independent of T_0, which is not satisfied for slowly diffusing species as Ganguly et al. (1998b) pointed out. To be applicable to a mineral with arbitrary extent of diffusion, the classical Dodson formulation (7) was modified by Ganguly and Tirone (1999). Remarkably, the modified formulation (see Eq. (14) of Ganguly and Tirone, 1999) has the same form as Eq. (7), whereas geometry factor A′ is a function of grain geometry, cooling rate, diffusion coefficient at the peak temperature, $D(T_0)$, and grain radius a (for details refer to Ganguly and Tirone, 1999).

When the T_C dependence on T_0 is taken into account, the deviations of T_C calculated using the modified Dodson formulation are becoming smaller with increasing peak temperature (T_0) and slower cooling rate (Ganguly et al., 1998b; Ganguly and Tirone, 1999). Fig. 9b and 9c show a comparison of the nominal "closure temperature" calculated from Eq. (7) with mean closure temperature for spherical grain of dry and hydrous garnet as a function of grain radius at a fixed cooling rate of 100 °C/Myr and different peak temperatures, using the extension of the Dodson formulation from Ganguly and Tirone (1999). It is evident that, for small grain radii and comparatively high peak temperatures, the mean closure temperature curves will converge upon the classical Dodson values, but significant deviations are expected for larger grains and lower peak temperatures. The potential for departure from these values, as outlined above in Fig. 9, should not be overlooked.

5. Conclusions

In this study, we have measured the Fe–Mg interdiffusion rates in garnet aggregates using the diffusion couple method at 3 GPa and 1373–1673 K. The effects of temperature, composition and water content on the diffusivity were investigated. Our results demonstrate that the composition of garnet has little influence on D_{Fe-Mg}, and the Fe–Mg inter-diffusivity in garnet containing 100–1260 wt. ppm H_2O is over two orders of magnitude faster than in anhydrous garnet at 1373 K. The extent of enhanced diffusivity by a small amount of water (100 wt. ppm) is almost identical to that associated with a 300 °C increase in temperature. Furthermore, the present diffusion experiments were carried out in the type-B kinetics regime, which suggests that the contribution of grain boundary diffusion to the total diffusive flux cannot be neglected based on the effective diffusion coefficients calculated. Finally, we calculated closure temperature, demonstrating that the role of water in modeling frozen compositional profiles for geospeedometry and geothermometry applications is much larger than previously considered.

Competing financial interests

The authors declare no competing financial interests.

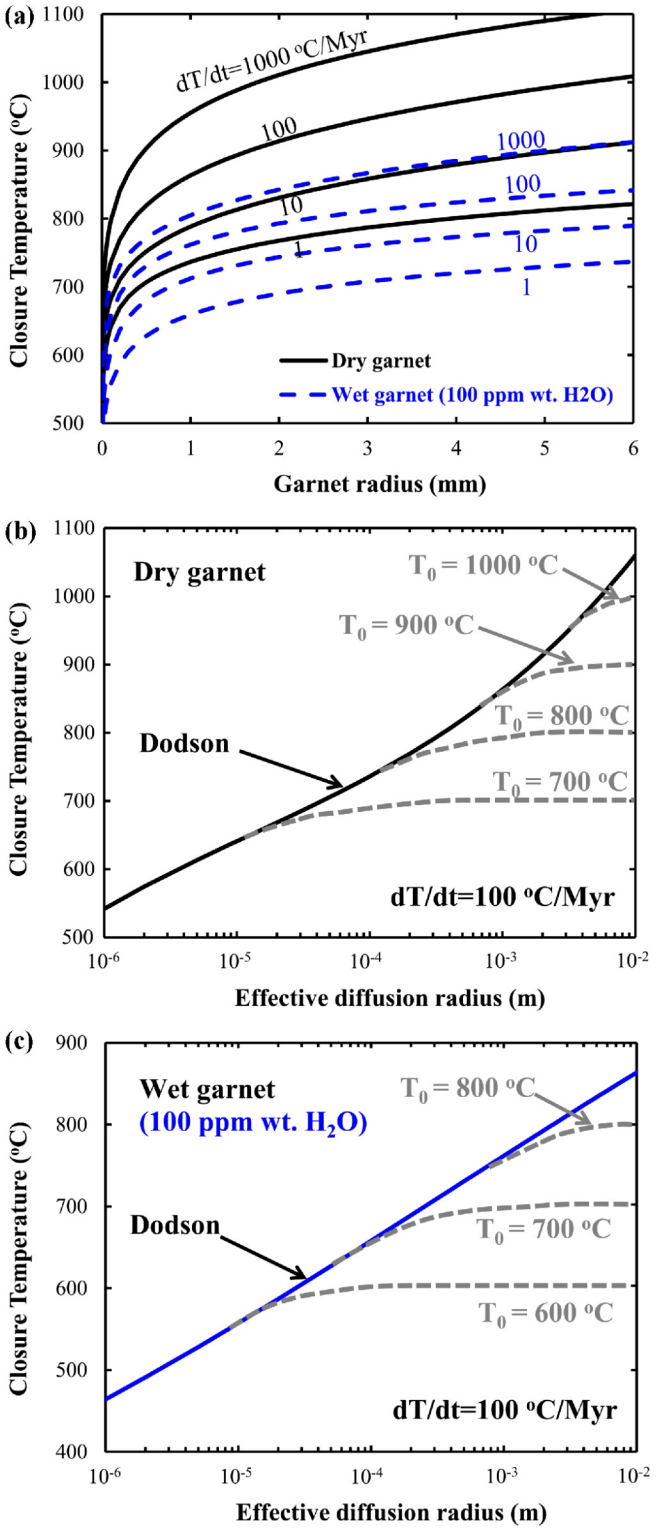

Fig. 9. (a) Closure temperature calculated for Fe–Mg interdiffusion in garnet as a function of grain radius for four different cooling rates, calculated using Dodson's classic expression (Eq. (7)) and diffusion parameters obtained in this study. Note that the *solid black* and *blue dashed lines* represent nominally dry and hydrous (100 wt. ppm H_2O) cases, respectively. Mean closure temperatures for Fe–Mg diffusion in garnet as a function of grain radius with a fixed cooling rate of 100 °C/Myr for dry (b) and hydrous cases with 100 ppm wt. H_2O (c), respectively. Closure temperature curves are calculated for a few different peak temperature (T_0), using the expressions of Ganguly and Tirone (1999). Also plotted are closure temperatures calculated using the classic Dodson formula (Dodson, 1973) (solid lines). Deviations in mean closure temperatures from the Dodson curves can be observed to increase with larger grain radii and decreasing peak temperatures. Spherical geometry was used in all calculations.

Acknowledgements

We thank Dr. D.J. Cherniak and two anonymous reviewers for their constructive comments that greatly improved the manuscript. Discussions with H.Z. Fei and D. Yamazaki helped to clarify some issues. We also appreciate the helps of Yang Li and Rui Li for characterization of diffusion couples. This work was supported by the Strategic Priority Research Program (B) of the Chinese Academy of Sciences (XDB 18010401), the 1000 Plan Program for Young Talents and Hundred Talent Program of CAS, NSF of China (41773056, 41303048) and Science Foundation of Guizhou Province (2017-1196, 2018-1176).

Appendix A. Supplementary material

Supplementary material related to this article can be found online at https://doi.org/10.1016/j.epsl.2018.10.015.

References

Borinski, S.A., Hoppe, U., Chakraborty, S., Ganguly, J., Bhowmik, S.K., 2012. Multicomponent diffusion in garnets I: general theoretical considerations and experimental data for Fe–Mg systems. Contrib. Mineral. Petrol. 164, 571–586.

Chakraborty, S., 1997. Rates and mechanisms of Fe–Mg interdiffusion in olivine at 980–1300 °C. J. Geophys. Res. 102 (B6), 12317–12331.

Chakraborty, S., Ganguly, J., 1992. Cation diffusion in alumino-silicate garnets: experimental determination in spessartine–almandine diffusion couples, evaluation of effective binary diffusion coefficients, and applications. Contrib. Mineral. Petrol. 111, 74–86.

Crank, J., 1975. The Mathematics of Diffusion, 2nd edition. Oxford University Press, London, pp. 1–414.

Dimanov, A., Wiedenbeck, M., 2006. (Fe, Mn)–Mg interdiffusion in natural diopside: effect of pO_2. Eur. J. Mineral. 18 (6), 705–718.

Dodson, M.H., 1973. Closure temperature in cooling geochronological and petrological systems. Contrib. Mineral. Petrol. 40, 259–274.

Dodson, M.H., 1986. Closure profiles in cooling systems. Mater. Sci. Forum 7, 145–154.

Dohmen, R., Heege, J.H., Becker, H.W., Chakraborty, S., 2016. Fe–Mg interdiffusion in orthopyroxene. Am. Mineral. 101, 2210–2221.

Dohmen, R., Milke, R., 2010. Diffusion in polycrystalline materials: grain boundaries, mathematical models, and experimental data. Rev. Mineral. Geochem. 72, 921–970.

Elphick, S.C., Ganguly, J., Loomis, T.P., 1985. Experimental determination of cation diffusivities in aluminosilicate garnets: I. Experimental methods and interdiffusion data. Contrib. Mineral. Petrol. 90, 36–44.

Faul, U.H., Cline, C.J., David, E.C., Berry, A.J., Jackson, I., 2016. Titanium-hydroxyl defect-controlled rheology of the Earth's upper mantle. Earth Planet. Sci. Lett. 452, 227–237.

Fei, H., Koizumi, S., Sakamoto, N., Hashiguchi, M., Yurimoto, H., Marquardt, K., Miyajima, N., Katsura, T., 2018. Mg lattice diffusion in iron-free olivine and implications to conductivity anomaly in the oceanic asthenosphere. Earth Planet. Sci. Lett. 484, 204–212.

Fei, H.Z., Wiedenbeck, M., Yamazaki, D., Katsura, T., 2013. Small effect of water on upper-mantle rheology based on silicon self-diffusion coefficients. Nature 498, 213–215.

Fei, H.Z., Wiedenbeck, M., Yamazaki, D., Katsura, T., 2014. No effect of water on oxygen self-diffusion rate in forsterite. J. Geophys. Res. 119 (10), 7598–7606.

Freer, R., Edwards, A., 1999. An experimental study of Ca–(Fe, Mg) interdiffusion in silicate garnets. Contrib. Mineral. Petrol. 134 (4), 370–379.

Ganguly, J., 2002. Diffusion kinetics in minerals: principles and applications to tectono-metamophic processes. EMU Notes Mineral. 4, 271–309.

Ganguly, J., Bhattacharya, R.N., Chakraborty, S., 1988. Convolution effect in the determination of compositional zoning by microprobe step scans. Am. Mineral. 73, 901–909.

Ganguly, J., Cheng, W., Chakraborty, S., 1998a. Cation diffusion in aluminosilicate garnets; experimental determination in pyrope–almandine diffusion couples. Contrib. Mineral. Petrol. 131, 171–180.

Ganguly, J., Tirone, M., 1999. Diffusion closure temperature and age of a mineral with arbitrary extent of diffusion: theoretical formulation and applications. Earth Planet. Sci. Lett. 170, 131–140.

Ganguly, J., Tirone, M., Hervig, R.L., 1998b. Diffusion kinetics of samarium and neodymium in garnet, and a method for determining cooling rates of rocks. Science 281, 805–807.

Gordon, R.S., 1985. Diffusional creep phenomena in polycrystalline oxides. In: Schock, R.N. (Ed.), Point Defects in Minerals. In: Geophys. Monogr., vol. 31. AGU, Washington, DC, pp. 132–140.

Harrison, L.G., 1961. Influence of dislocations on diffusion kinetics in solids with particular reference to the alkali halides. Trans. Faraday Soc. 57, 1191–1199.

Hier-Majumder, S., Anderson, I.M., Kohlstedt, D.L., 2005. Influence of protons on Fe–Mg interdiffusion in olivine. J. Geophys. Res. 110, B02202.

Irifune, T., Ringwood, A.E., 1987. Phase transformations in primitive MORB and pyrolite compositions to 25 GPa and some geophysical implications. In: High-Pressure Research in Mineral Physics: A Volume in Honor of Syun-iti Akimoto, pp. 231–242.

Joesten, R., 1991. Grain-boundary diffusion kinetics in silicate and oxide minerals. In: Ganguly, J. (Ed.), Diffusion, Atomic Ordering, and Mass Transport: Selected Problems in Geochemistry. Springer-Verlag, New York, pp. 345–395.

Katayama, I., Hirose, K., Yurimoto, H., Nakashima, S., 2003. Water solubility in majoritic garnet in subducting oceanic crust. Geophys. Res. Lett. 30 (22), 2155.

Kubo, T., Shimojuko, A., Ohtani, E., 2004. Fe–Mg interdiffusion rates in wadsleyite and the diffusivity jump at the 410 km discontinuity. Phys. Chem. Miner. 31, 456–464.

Li, B.W., Ge, J.H., Zhang, B.H., 2018. Diffusion in garnet: a review. Acta Geochim. 37 (1), 19–31.

Mackwell, S.J., Bystricky, M., Sproni, M., 2005. Fe–Mg interdiffusion in (Mg, Fe)O. Phys. Chem. Miner. 32 (5–6), 418–425.

Matano, C., 1933. On the relation between the diffusion coefficients and concentrations of solid metals (the nickel–copper system). Jpn. J. Phys. 8, 109–113.

Mei, S., Kohlstedt, D.L., 2000. Influence of water on plastic deformation of olivine aggregates: 1. Diffusion creep regime. J. Geophys. Res. 105 (B9), 21457–21469.

Mendelson, M.I., 1969. Average grain size in polycrystalline ceramics. J. Am. Ceram. Soc. 52, 443–446.

Mirwald, P.W., Massonne, H.J., 1980. The low-high quartz and quart-coesite transition to 40 kbar between 600° and 1600 °C and some reconnaissance data on the effect of $NaAlO_2$ component on the low quartz-coesite transition. J. Geophys. Res. 85 (B12), 6983–6990.

Mookherjee, M., Karato, S., 2010. Solubility of water in pyrope-rich garnet at high pressures and temperatures. Geophys. Res. Lett. 37, L03310.

Müller, T., Dohmen, R., Becker, H.W., ter Heege, J.H., Chakraborty, S., 2013. Fe–Mg interdiffusion rates in clinopyroxene: experimental data and implications for Fe–Mg exchange geothermometers. Contrib. Mineral. Petrol. 166, 1563–1576.

Otsuka, K., Karato, S., 2015. The influence of ferric iron and hydrogen on Fe–Mg interdiffusion in ferropericlase (Mg, Fe)O in the lower mantle. Phys. Chem. Miner. 42 (4), 261–273.

Paterson, M.S., 1982. The determination of hydroxyl by infrared absorption in quartz, silicate glasses and similar materials. Bull. Minéral. 105, 20–29.

Perchuk, A.L., Burchard, M., Schertl, H.P., Maresch, W.V., Gerya, T.V., Bernhardt, H.J., Vidal, O., 2009. Diffusion of divalent cations in garnet. Contrib. Mineral. Petrol. 157, 573–592.

Pigott, J.S., Wright, K., Gale, J.D., Panero, W.R., 2015. Calculation of the energetics of water incorporation in majorite garnet. Am. Mineral. 100, 1065–1075.

Raj, R., Ashby, M.F., 1971. On grain boundary sliding and diffusional creep. Metall. Trans. 2, 1113–1127.

Schwandt, C.S., Cygan, R.T., Westrich, H.R., 1995. Mg self-diffusion in pyrope garnet. Am. Mineral. 80, 483–490.

Shtukenberg, A.G., Popov, D.Y., Punin, Y.O., 2005. Growth ordering and anomalous birefringence in ugrandite garnets. Mineral. Mag. 69 (4), 537–550.

Vielzeuf, D., Baronnet, A., Perchuk, A.L., Laporte, D., Baker, M.R., 2007. Calcium diffusivity in alumino-silicate garnets: an experimental and ATEM study. Contrib. Mineral. Petrol. 154, 153–170.

Vogt, K., Dohmen, R., Chakraborty, S., 2015. Fe–Mg diffusion in spinel: new experimental data and a point defect based model. Am. Mineral. 100, 2112–2122.

Wang, D.J., Mookherjee, M., Xu, Y.S., Karato, S., 2006. The effect of water on the electrical conductivity in olivine. Nature 443, 977–980.

Wright, K., Freer, R., Catlow, C.R.A., 1994. The energetics and structure of the hydrogarnet defect in grossular: a computer simulation study. Phys. Chem. Miner. 20, 500–503.

Xia, Q.K., Sheng, Y.M., Yang, X.Z., Yu, H.M., 2005. Heterogeneity of water in garnets from UHP eclogites, eastern Dabieshan, China. Chem. Geol. 224 (4), 237–246.

Xu, L.L., Mei, S.H., Dixon, N., Jin, Z.M., Suzuki, A.M., Kohlstedt, D.L., 2013. Effect of water on rheological properties of garnet at high temperatures and pressures. Earth Planet. Sci. Lett. 379, 158–165.

Yamazaki, D., Irifune, T., 2003. Fe–Mg interdiffusion in magnesiowüstite up to 35 GPa. Earth Planet. Sci. Lett. 216, 301–311.

Yang, X.Z., 2012. Orientation-related electrical conductivity of hydrous olivine, clinopyroxene and plagioclase and implications for the structure of the lower continental crust and uppermost mantle. Earth Planet. Sci. Lett. 317–318, 241–250.

Yoshino, T., Matsuzaki, T., Yamashita, S., Katsura, T., 2006. Hydrous olivine unable to account for conductivity anomaly at the top of the asthenosphere. Nature 443, 973–976.

Zhang, B.H., 2017. An overview of Fe–Mg interdiffusion in mantle minerals. Surv. Geophys. 38, 727–755.

Zhang, B.H., Yoshino, T., Wu, X.P., Matsuzaki, T., Shan, S., Katsura, T., 2012. Electrical conductivity of enstatite as a function of water content: implications for the electrical structure in the upper mantle. Earth Planet. Sci. Lett. 357–358, 11–20.